A nonlinear gradient elasticity model for the prediction of seismic waves

Leo Dostal*, Marten Hollm*, Andrei V. Metrikine†, Andrei B. Fărăgău† and Karel N. van Dalen†
**Institute of Mechanics and Ocean Engineering, Hamburg University of Technology, Hamburg, Germany*
†Faculty of Civil Engineering & Geosciences, TU Delft, Delft, Netherlands

Summary. We present a novel equation of motion for a nonlinear gradient elasticity model. Thereby, higher-order gradient terms are introduced to capture the effect of small-scale soil heterogeneity/micro-structure. Using a newly established finite difference scheme, corresponding solutions including stationary waves are determined. In comparison with a commonly used model for nonlinear seismic waves, which has leading derivatives of second order, the solutions of the novel equations are much smoother. This allows much more accurate numerical computations as well as more realistic predictions of the seismic waves.

Introduction

In order to predict the response of the top soil layers of the earth - the so-called seismic site response- induced by seismic waves, the so-called equivalent linear scheme is used very often. Thereby, soil stiffness and damping are modeled taking a shear modulus and material damping ratio, which are constant in time [1]. However, for high maximum strain levels in the soil layers, the equivalent linear scheme with constant shear modulus and material damping can not adequately represent the behavior of a seismic event over its entire duration, since the strains in the soil layers vary significantly. In order to account for the variation of shear modulus and damping ratio in this case, a nonlinear time domain solution is usually used, e.g. [2].
Actual research in nonlinear modeling for seismic site response is mostly focused on the development of advanced constitutive models, which capture important features of the soil behavior like anisotropy, pore water pressure generation and dilation [3]. In this work, we determine specific solutions including stationary waves in the subsurface, whereby the constitutive behavior is governed by the hyperbolic soil model. Here, the (secant) shear modulus is strain dependent with a non-polynomial nonlinearity. In order to capture the effects of small-scale heterogeneity/ micro-structure, we extend the classical wave equation to a nonlinear gradient elasticity model. This is sometimes also called a higher-order gradient continuum or a micro-structured solid. Compared to the classical continuum, higher-order gradient terms are introduced into the equation of motion, which lead to dispersive effects particularly for shorter waves [4]. These higher-order gradient terms are usually obtained using asymptotic homogenization techniques for periodically inhomogeneous media [4]. Since localized stationary waves exist only because of the balance between dispersive and nonlinear effects, their influence on the behavior of stationary solutions is significant and allows them to propagate without distortion. Since the dispersion prohibits the formation of jumps, physically realizable solutions are obtained.
In this work, the effects of the higher-order gradient terms and the corresponding dispersion are investigated. Thereby, specific solutions of the corresponding equations of motion are presented and compared. It is observed that the classical wave equation contains solutions which have non-physical discontinuities (in the strain) and which vanish in the presence of the higher-order terms.
The structure of this work is as follows: First, we derive the equation of motion of the classical and nonlinear gradient elasticity model, respectively. The derivation is based on Newton's second law and Eringen's general strain-stress relation [5]. Then, an ordinary differential equation is derived, from which stationary solutions for the nonlinear gradient elasticity model are obtained. Afterwards, a numerical scheme for the computation of the derived nonlinear equations of motion in time and space is presented. Using this scheme, solutions of the classical and nonlinear gradient elasticity model are compared. Finally, this work ends with a conclusion.

Model

In this section, a classical and an advanced constitutive model are described in order to capture important features of the soil behavior, respectively. In both cases, the constitutive behavior is governed by the hyperbolic soil model, which results in a strain-dependent shear modulus. As the classical model has non-physical discontinuous solutions, a nonlinear gradient elasticity model is employed.

The classical continuum model

In order to derive the equation of motion, Newton's second law is applied. Let x be the horizontal direction, z the vertical direction and t the time. For transverse waves propagating in the direction of z and considering the one-dimensional situation, it reads [6]

$$\rho \frac{\partial^2 u}{\partial t^2} = \frac{\partial \sigma_{zx}}{\partial z}. \tag{1}$$

Thereby, $u(z,t)$ is the displacement in x, σ_{zx} is the shear stress and ρ is the material density. The corresponding strain can be calculated from the displacement by [6]

$$\varepsilon_{zx} = \frac{1}{2}\frac{\partial u}{\partial z}. \tag{2}$$

In this study, the constitutive behavior is governed by the hyperbolic soil model, which is typically employed for the seismic site response analysis. Here, the strain-dependent shear modulus [7]

$$G(\gamma) = \frac{G_0}{1 + (\gamma/\gamma_{\text{ref}})^{\beta}} \quad \text{with} \quad \gamma = \sqrt{3}|\varepsilon_{zx}| = \frac{\sqrt{3}}{2}\left|\frac{\partial u}{\partial z}\right| \tag{3}$$

is used, whereby γ_{ref} denotes the reference shear strain and $0 < \beta < 1$ is a dimensionless constant. Applying the stress-strain relationship

$$\sigma_{zx} = 2\,G(\gamma)\,\varepsilon_{zx}, \tag{4}$$

Eq. (1) results in

$$\rho\frac{\partial^2 u}{\partial t^2} = \frac{\partial}{\partial z}\left(G(\gamma)\frac{\partial u}{\partial z}\right). \tag{5}$$

This is the wave equation for the classical continuum model.

The nonlinear gradient elasticity model

In order to capture the effects of small-scale soil heterogeneity/micro-structure, the stress strain relationship of Eq. (4) is extended by including higher-order gradient terms. In a nonlinear system, the stress-strain relation can generally be written as [5]

$$\sigma_{zx}(z,t) = \int_{-\infty}^{\infty}\int_{-\infty}^{\infty} g\left(z-\zeta, t-\tau, \gamma(\zeta,\tau)\right)\varepsilon_{zx}(\zeta,\tau)\,\mathrm{d}\zeta\mathrm{d}\tau, \tag{6}$$

whereby the kernel function $g(z,t,\gamma)$ contains the specific nonlocality and history dependence. In order to compute the soil behavior using a partial differential equation instead of an integro-differential equation, the kernel function is taken as a combination of Dirac delta functions $\delta(\ldots)$. This results in [8]

$$g(z-\zeta, t-\tau, \gamma) = 2\big(G(\gamma)\delta(z-\zeta)\delta(t-\tau) - L^2G^{(L)}(\gamma)\delta_{,\zeta\zeta}(z-\zeta)\delta(t-\tau) + T^2G^{(T)}(\gamma)\delta(z-\zeta)\delta_{,\tau\tau}(t-\tau)\big). \tag{7}$$

Thereby, $(\ldots)_{,\zeta\zeta}$ and $(\ldots)_{,\tau\tau}$ denote double partial differentiation with respect to ζ and τ, respectively. Apart from the conventional strain-dependent shear modulus $G(\gamma)$, the kernel function g contains additional strain-dependent elastic moduli $G^{(L)}(\gamma)$ and $G^{(T)}(\gamma)$, respectively. Finally, L and T are time and length scales which specify the nonlocality and history dependence of the medium, respectively.
Without loss of generality, the scales T and L are interrelated in this work by $T^2 = L^2/c_0^2$, whereby $c_0 = \sqrt{G_0/\rho}$ is the shear wave speed corresponding to the small-strain shear modulus G_0 from linear elasticity.
For simplicity, the additional elastic moduli are related to the conventional strain-dependent shear modulus $G(\gamma)$ by

$$G^{(L)}(\gamma) = B_1G(\gamma), \quad G^{(T)}(\gamma) = B_2G(\gamma). \tag{8}$$

Thereby, B_1 and B_2 are dimensionless constants. Inserting Eqs. (2), (6), (7) and (8) into (1) results into

$$\rho\frac{\partial^2 u}{\partial t^2} = \frac{\partial}{\partial z}\left(G(\gamma)\frac{\partial u}{\partial z} - B_1L^2\frac{\partial^2}{\partial z^2}\left(G(\gamma)\frac{\partial u}{\partial z}\right) + B_2\frac{\rho L^2}{G_0}\frac{\partial^2}{\partial t^2}\left(G(\gamma)\frac{\partial u}{\partial z}\right)\right). \tag{9}$$

This is the equation of motion of the nonlinear gradient elasticity model used in this work. A comparison of Eq. (9) with Eq. (5) shows that the effects of small-scale soil heterogeneity/micro-structure are accounted for by the higher-order gradient terms multiplied with B_1 and B_2, respectively.
In this work, the hyperbolic soil model $G(\gamma)$ given in Eq. (3) is also used for the nonlinear gradient elasticity model.

Stationary wave solution

In the following, the influence of the higher-order gradient terms on the behavior of numerical solutions is considered. Thereby, stationary solutions of Eq. (9) are taken considered. These solutions can be determined by assuming that they propagate with constant speed $c \in \mathbb{R}$ through the nonlinear medium while not changing their shape [8]. Applying the transformation $\xi = x - ct$ and assuming stationarity, this results in

$$u_{,tt} = u_{,\xi\xi}c^2, \quad u_{,ztt} = u_{,\xi\xi\xi}c^2, \quad u_{,zt} = -u_{,\xi\xi}c, \quad \frac{\partial}{\partial z} = \frac{\partial}{\partial \xi}. \tag{10}$$

Computing the derivatives of $G(\gamma)u_{,\xi}$ with respect to ξ, we get for $y := u_{,\xi}$ [8]

$$
\begin{aligned}
y_{,\xi\xi} =& \frac{1}{1-\beta\left(\frac{\sqrt{3}|y|}{2\gamma_{\mathrm{ref}}}\right)^{\beta}\left(1+\left(\frac{\sqrt{3}|y|}{2\gamma_{\mathrm{ref}}}\right)^{\beta}\right)^{-1}}\Bigg\{\frac{\rho c^2\left(1+\left(\frac{\sqrt{3}|y|}{2\gamma_{\mathrm{ref}}}\right)^{\beta}\right)-G_0}{B_2c^2\rho L^2-G_0B_1L^2}y \\
&-\frac{\sqrt{3}\,\mathrm{sgn}(y)}{2\gamma_{\mathrm{ref}}}\left[2\beta^2\left(\frac{\sqrt{3}|y|}{2\gamma_{\mathrm{ref}}}\right)^{2\beta-1}\left(1+\left(\frac{\sqrt{3}|y|}{2\gamma_{\mathrm{ref}}}\right)^{\beta}\right)^{-2}\right. \\
&\left.-(\beta+\beta^2)\left(\frac{\sqrt{3}|y|}{2\gamma_{\mathrm{ref}}}\right)^{\beta-1}\left(1+\left(\frac{\sqrt{3}|y|}{2\gamma_{\mathrm{ref}}}\right)^{\beta}\right)^{-1}\right]y_{,\xi}^2\Bigg\}.
\end{aligned}
\tag{11}
$$

Solving this nonlinear second-order ordinary differential equation, stationary wave solutions of Eq. (9) can be computed.

Numerical scheme for the nonlinear gradient elasticity model

In order to compute the corresponding numerical solutions $u(z,t)$ of Eqn. (5) and (9), a numerical scheme based on finite-difference approximations is used. This scheme has been developed by Dostal et al. [8] and solves partial differential equations of the form

$$
\rho\frac{\partial^2 u}{\partial t^2}=\frac{\partial}{\partial z}\left(G\left(\frac{\partial u}{\partial z}\right)\frac{\partial u}{\partial z}-B_1L^2\frac{\partial^2}{\partial z^2}\left(G\left(\frac{\partial u}{\partial z}\right)\frac{\partial u}{\partial z}\right)+B_2\frac{\rho L^2}{G_0}\frac{\partial^2}{\partial t^2}\left(G\left(\frac{\partial u}{\partial z}\right)\frac{\partial u}{\partial z}\right)\right). \tag{12}
$$

Thereby, $G\left(\frac{\partial u}{\partial z}\right)$ is an arbitrary function depending on $\frac{\partial u}{\partial z}$. If $G\left(\frac{\partial u}{\partial z}\right)$ is chosen as in Eq. (3), Eq. (12) reduces to Eq. (9). If furthermore B_1 and B_2 are set to zero, Eq. (12) becomes Eq. (5). Since all numerical results presented in the next section are based on the scheme developed in [8], we briefly outline it here.

It is assumed that the analytical solution $u(z,t)$ of Eq. (12) exists in space $z \in [Z_\ell, Z_h]$ and time $t \in [0, \mathbb{T}]$. Therefore, a grid in space

$$
Z_\ell = z_0 < z_1 < \cdots < z_M = Z_h, \quad z_i = i\Delta z \;\text{ for } i = 0,\ldots,M,\; \Delta z = \frac{Z_\ell - Z_h}{M}, \tag{13}
$$

and time

$$
0 = t_0 < t_1 < \cdots < t_N = \mathbb{T}, \quad t_n = n\Delta t \;\text{ for } n = 0,\ldots,N,\; \Delta t = \frac{\mathbb{T}}{N}, \tag{14}
$$

is introduced, respectively. Defining

$$
h(u_{,z}) := G(u_{,z})\,u_{,z}, \tag{15}
$$

Eq. (12) becomes

$$
\rho\,u_{,tt} = h_{,z} - B_1L^2h_{,zzz} + B_2\frac{\rho L^2}{G_0}h_{,ttz}. \tag{16}
$$

In this way, the structure of the considered partial differential equation is exploited. As will be seen later, this simplifies the calculation of the spatial finite difference approximations.

In order to approximate the derivatives with respect to time, it is assumed that the solution is known at the timepoints t_{n-1} and t_n. Let u_i^n be a grid function, which approximates the analytical solution u at space z_i and time t_n, i. e. $u_i^n \approx u(z_i,t_n)$. Furthermore, let $u_{i,z}^n$ be a grid function approximating $u_{,z}(z_i,t_n)$. Replacing the time derivative with a finite difference approximation, Eq. (12) yields

$$
\mathbf{f}(\mathbf{u}^{n+1}) = \mathbf{0} \;\text{ with } \mathbf{u}^{n+1} := \left[u_0^{n+1}, u_1^{n+1}, \ldots, u_M^{n+1}\right]^{\mathrm{T}}, \tag{17}
$$

whereby

$$
\begin{aligned}
f_i(\mathbf{u}^{n+1}) :=& \rho\,\frac{u_i^{n+1}-2u_i^n+u_i^{n-1}}{\Delta t^2}-\frac{h_{,z}(u_{i,z}^{n+1})+2h_{,z}(u_{i,z}^{n})+h_{,z}(u_{i,z}^{n-1})}{4} \\
&+B_1L^2\frac{h_{,zzz}(u_{i,z}^{n+1})+2h_{,zzz}(u_{i,z}^{n})+h_{,zzz}(u_{i,z}^{n-1})}{4}-B_2\frac{\rho L^2}{G_0}\frac{h_{,z}(u_{i,z}^{n+1})-2h_{,z}(u_{i,z}^{n})+h_{,z}(u_{i,z}^{n-1})}{\Delta t^2}.
\end{aligned}
\tag{18}
$$

A solution of Eq. (18) approximates the corresponding exact solution of Eq. (12) up to an accuracy of $\mathcal{O}(\Delta t^2)$.

Next, the space derivatives $h_{,z}(u_{i,z})$ and $h_{,zzz}(u_{i,z})$ at location $z = z_i$ are approximated. Thereby, the following standard finite differences are used, which have all an accuracy of $\mathcal{O}(\Delta z^2)$:

$$
\begin{aligned}
u_{i,z} &= \frac{u_{i+1}-u_{i-1}}{2\Delta z}+\mathcal{O}(\Delta z^2), \quad h_{,z}(u_{i,z}) = \frac{h(u_{i+1,z})-h(u_{i-1,z})}{2\Delta z}+\mathcal{O}(\Delta z^2), \\
h_{,zzz}(u_{i,z}) &= \frac{h(u_{i+2,z})-2h(u_{i+1,z})+2h(u_{i-1,z})-h(u_{i-2,z})}{2\Delta z^3}+\mathcal{O}(\Delta z^2).
\end{aligned}
\tag{19}
$$

In order to simplify the notation, the time index n is omitted. If the hyperbolic soil model $G(u_{,z})$ from Eq. (3) is used, we get for $h_{,z}$:

$$\begin{aligned} h_{,z}(u_{i,z}) =& \frac{h(u_{i+1,z}) - h(u_{i-1,z})}{2\Delta z} + \mathcal{O}(\Delta z^2) \\ =& \frac{1}{2\Delta z}\left\{ \frac{G_0}{1+\left(\frac{\sqrt{3}}{2}\frac{|u_{i+2}-u_i|}{2\Delta z \gamma_{\text{ref}}}\right)^\beta} \frac{u_{i+2}-u_i}{2\Delta z} - \frac{G_0}{1+\left(\frac{\sqrt{3}}{2}\frac{|u_i-u_{i-2}|}{2\Delta z \gamma_{\text{ref}}}\right)^\beta} \frac{u_i - u_{i-2}}{2\Delta z} \right\} + \mathcal{O}(\Delta z^2). \end{aligned} \tag{20}$$

The approximation of $h_{,zzz}$ follows analogously.
Now the advantage of the presented numerical scheme can be seen: In Eq. (12), the third-order space derivative of $G(u_{,z})$ has to be computed. However, since the hyperbolic soil model defined in Eq. (3) contains the absolute value function $k(x) = |x|$, the function $G(u_{,z})$ is only one time weakly differentiable. By introducing the function h, the problem of the missing differentiability is circumvented.
With this, the solution $\mathbf{u}^{n+1}$ of $\mathbf{f}(\mathbf{u}^{n+1}) = \mathbf{0}$ can be computed solving a nonlinear system of equations. This can be done iteratively using Newton's method, for example.

Numerical results

In this section, numerical results for the nonlinear Eqs. (5) and (9) are shown. Corresponding results are compared in order to investigate the effects of the higher-order gradient terms. Thereby, the parameters from Table 1 are used. While the values of G_0, ρ, β and γ_{ref} have been chosen to represent soil, the values of B_1 and B_2 are similar to the ones used in [4].

Table 1: Medium parameter values.

G_0 [Pa]	ρ $\left[\mathrm{kg\,m^{-3}}\right]$	β [-]	γ_{ref} [-]	B_1 [-]	B_2 [-]	L [m]
$111.86 \cdot 10^6$	2009.8	0.91	10^{-3}	1	1.78	0.2

Solutions of a Gaussian pulse

First of all, the effects of the higher-order gradient terms are studied for a specific solution, where as initial condition a Gaussian pulse is used:

$$u(z, t = 0) = u_0 \exp\left(-\frac{z^2}{2\sigma^2}\right). \tag{21}$$

Here, the amplitude of the pulse is set to $u_0 = 0.0016$ m and the standard deviation is set to $\sigma = 1$ m. In accordance with [2], these values are chosen to obtain a relatively high strain level. The temporal evolution of the numerical solution is computed using the scheme described in the last section, whereby absorbing boundary conditions are applied. Thereby, an additional initial condition u^{-1} at time t_{-1} has to be chosen. In this study, $u^{-1} = u^0$ is used, which results in a solution with no initial velocity.
The resulting solution of Eq. (5) can be seen in Fig. 1. It is observed that the initial pulse divides into two parts, which travel in opposite directions. Furthermore, the numerical solution of the classical model is non-smooth due to the sharp edges (one at the top of the wave and the other at the bottom behind it). This makes the strain discontinuous at those locations, which is not physically admissible. In contrast to this, Fig. 2 shows the corresponding solution of Eq. (9), where the effect of higher-order gradient terms are taken into account. Again, a solution is shown where the initial pulse is divided into two parts. However, the shape of the solution is smoother and does not contain sharp edges. Instead of sharp edges, small oscillations are observed behind the wave, which is consistent with the findings in [4]. This can also be seen in Fig. 3, which shows the corresponding solutions at the end of the simulation time together with the used initial condition. By introducing dispersion, the higher-order gradient terms lead to a solution where sharp edges do not occur and therefore lead to a physically admissible behavior.
Moreover, Fig. 3 shows that after division, both solutions travel with the same speed. Furthermore, a negative displacement is observed at $z = 0$ m after the initial pulse has departed. This could be caused by the combination of the hyperbolic soil model with the Gaussian pulse that has non-zero content at zero wavenumber. However, this shift in negative direction decreases for increasing time. This is shown in Fig. 4, which shows the solution at $z = 0$ m over time.

Stationary solution of the nonlinear gradient elasticity model

Next, the effects of the higher-order gradient terms on the stationary solution of Eq. (9) are investigated. For this, Eq. (11) is computed for the velocity $c = 100$ m/s. Since the numerical scheme of the last section needs an additional initial condition u^{-1} at t_{-1}, the corresponding value has to be calculated. As the stationary solution propagates with speed c, the value of u^{-1} is computed by shifting u^0 in space by ct_{-1}. Since the solution of Eq. (11) is periodic in space, periodic boundary conditions are used to calculate the temporal evolution of the solutions of Eqs. (9) and (5), respectively.
From Eq. (11), the corresponding phase portrait for u_ξ and $u_{\xi\xi}$ can be obtained. In the following, we study solutions where the trajectories approximate the homoclinic orbit. Using the solution of Eq. (11) as initial condition, the resulting

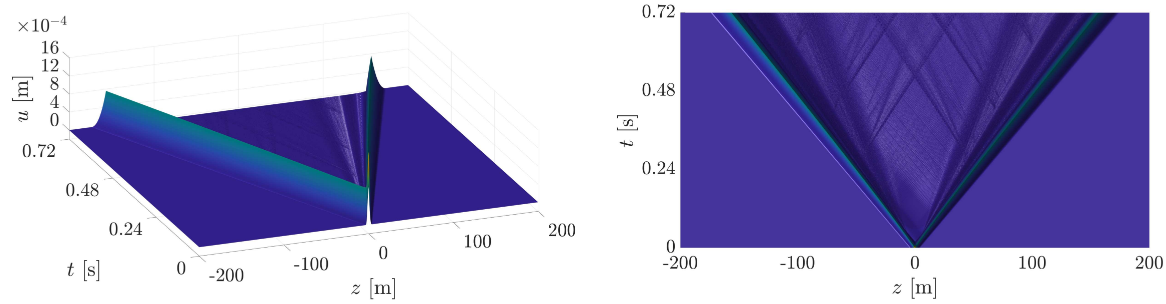

Figure 1: Numerical solution of Eq. (5) for the classical model. Thereby, a Gaussian pulse is chosen as initial condition. The solution is shown from two different perspectives.

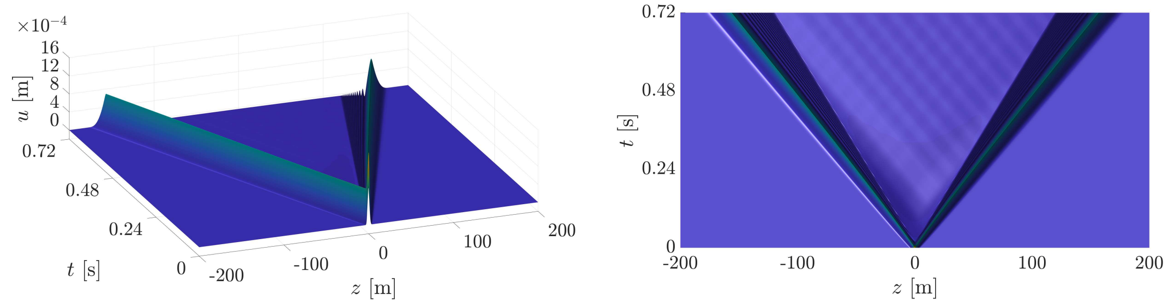

Figure 2: Numerical solution of Eq. (9) for the higher-order elasticity model. Thereby, a Gaussian pulse is chosen as initial condition. The solution is shown from two different perspectives.

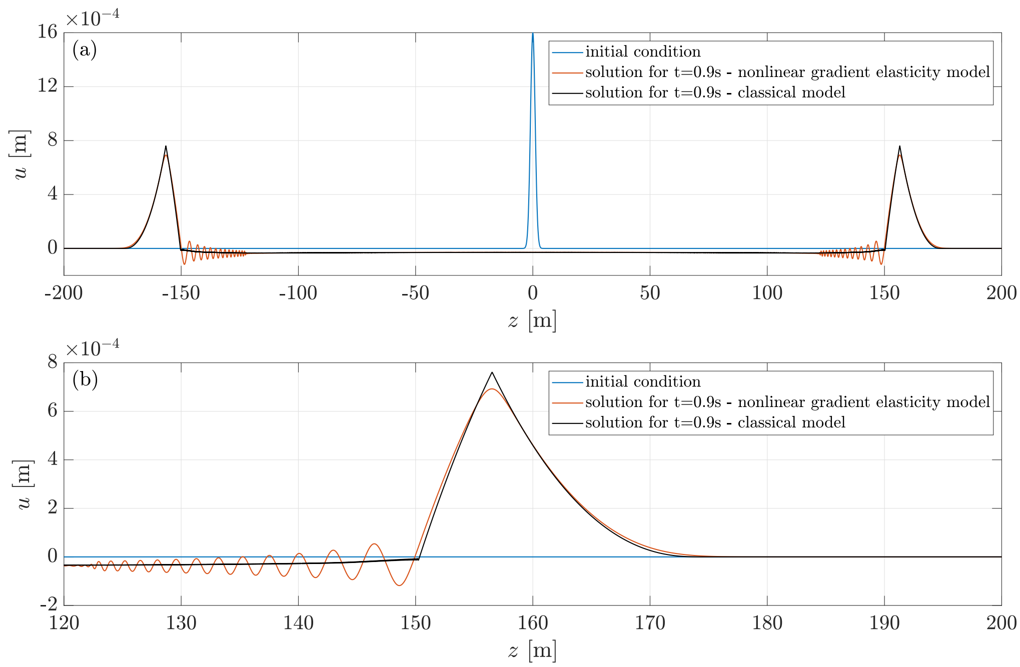

Figure 3: Comparison of the numerical solutions of Eqn. (5) and (9) at the end of the simulation time. In both cases, the Gaussian pulse is used as initial condition. The solution is shown for (a) $z \in [-200\,\mathrm{m},\ 200\,\mathrm{m}]$ and (b) $z \in [120\,\mathrm{m},\ 200\,\mathrm{m}]$, respectively.

solution of Eq. (9) is shown in Fig. 5. It is shown that the solution consists of two plateaus with different heights, which are alternating in space. As the shape of the solution is not changing in time, this is truly a stationary solution.

In order to investigate the effects of the higher-order gradient terms on the stationary solution, Fig. 6 shows the solution of Eq. (5). Thereby, the same initial condition as in Fig. 5 is used. It can be seen that high disturbances are introduced into the temporal evolution of the solution. These disturbances have their spatial origin in the transition area between the two plateaus of the initial condition, where high derivatives occur. They move in the opposite direction to the corresponding stationary solution.

Moreover, Fig. 7 compares the corresponding solutions at the end of the simulation time. It is observed that the higher-order-gradient terms and the disturbance shown in Fig. 6 change the shape of the solution. This shows that the dispersive effects influence the behavior of localized stationary solutions significantly, as they only exist exactly due to the balance

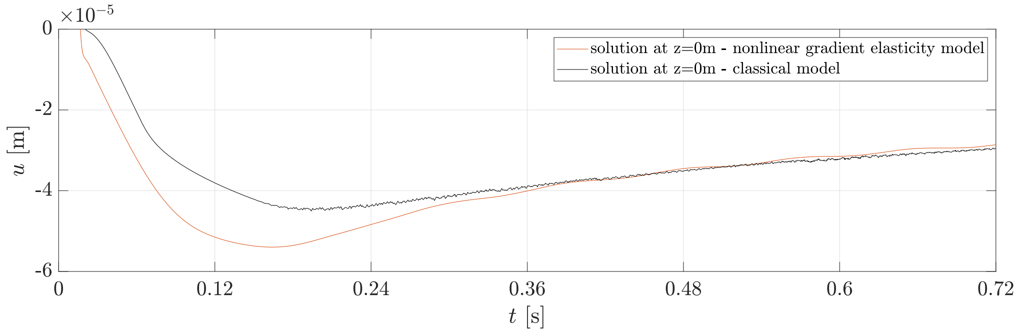

Figure 4: Comparison of the numerical solutions of Eqn. (5) and (9) at $z = 0\,\text{m}$. In both cases, the Gaussian pulse is used as initial condition.

of nonlinear and dispersive effects. Once the dispersive terms are removed, the stationary solution can no longer exist. It has to be noted that oscillations of very small wavelength occur in the solution of Eq. (5). These are arising due to the large values of the derivatives, which lead to numerical inaccuracies. However, these inaccuracies have such a small effect on the solution behavior that they do not destroy the structure of the solution.

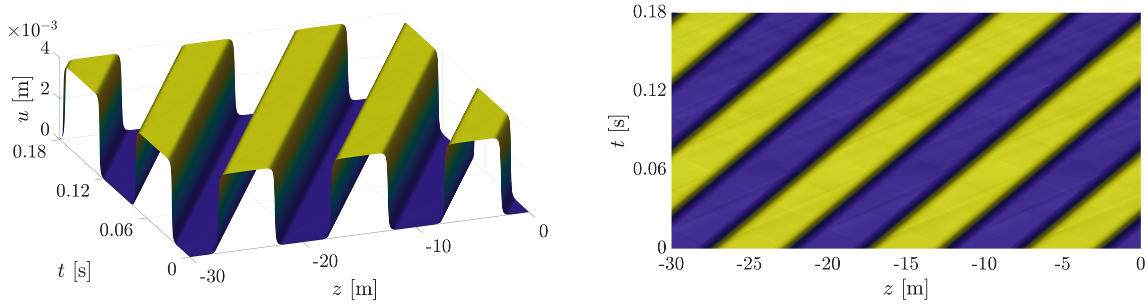

Figure 5: Numerical solution of Eq. (9) for the higher-order elasticity model. Thereby, the stationary solution of Eq. (11) is chosen as initial condition. The solution is shown from two different perspectives.

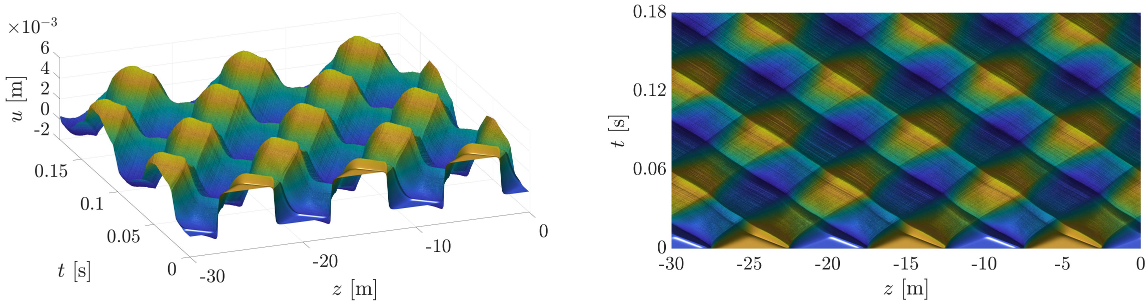

Figure 6: Numerical solution of Eq. (5) for the classical model. Thereby, the stationary solution of Eq. (11) is chosen as initial condition. The solution is shown from two different perspectives.

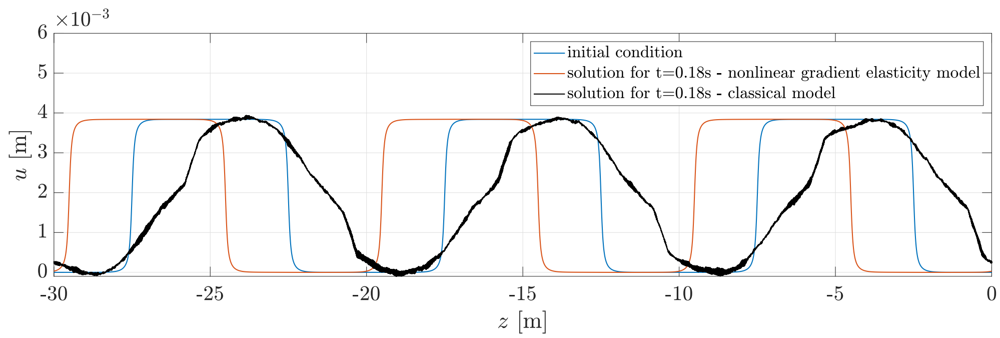

Figure 7: Comparison of the numerical solutions resulting from Eqn. (5) and (9) at the end of the simulation time. In both cases, the stationary solution of Eq. (11) is used as initial condition.

Conclusions

The response of the top layers of the earth induced by seismic waves is investigated. In this study, the constitutive behavior is governed by the hyperbolic soil model, whereby the shear modulus is strain dependent. The effects of small-scale heterogeneity/micro-structure is captured by considering higher-order gradient terms, which introduce dispersive effects. These effects are investigated in this work. For this, the corresponding equations of motion are solved using a numerical scheme, which has been introduced in Dostal et al. [8]. This scheme exploits the structure of the equation of motion and provides an accuracy of $\mathcal{O}(\Delta t^2 + \Delta z^2)$ in time and space.
Having applied this scheme using the Gaussian pulse as initial condition, it is shown that the higher-order gradient terms prohibit the formation of jumps. In this way, they lead to physically realizable solutions.
Moreover, the effects of the higher-order gradient terms are studied for the stationary solution of the equation of motion. Here, it is shown that the dispersive effects influence the behavior of localized stationary solutions significantly, as they only exist exactly due to the balance of nonlinear and dispersive effects. Once the dispersive terms are removed, the stationary solution can no longer exist.
In conclusion, this work shows that the proposed nonlinear gradient elasticity model provides physically realizable solutions. The introduced higher-order gradient terms are necessary and have significant influence on the corresponding solutions.

References

[1] Rodriguez-Marek A., Kruiver P.P., Meijers P., Bommer J.J., Dost B., van Elk J., Doornhof D. (2017) A Regional Site-Response Model for the Groningen Gas Field. *Bull. Seismol. Soc. Am.* **107**:2067–2077.

[2] Régnier J., Bonilla L.-F., Bard P.-Y., Bertrand E., Hollender F., Kawase H., Sicilia D., Arduino P., Amorosi A., Asimaki D., et al. (2016): International Benchmark on Numerical Simulations for 1D, Nonlinear Site Response (PRENOLIN): Verification Phase Based on Canonical Cases. *Bull. Seismol. Soc. Am.* **106**:2112–2135.

[3] Hashash Y.M.A., Phillips C., Groholski D.R. (2010) Recent Advances in Non–Linear Site Response Analysis. In: The 5th International Conference in Recent Advances in Geotechnical Eartqhuake Engineering and Soil Dynamics, San Diego, CA.

[4] Metrikine A. (2006) On causality of the gradient elasticity models. *J. Sound Vib.* **297**:727–742.

[5] Eringen A.C. (2002) Nonlocal Continuum Field Theories. Springer, NY.

[6] Verruijt A. (2009) An Introduction to Soil Dynamics. Vol. 24, Springer, New York

[7] Hardin B. O., Drnevich V. P. (1972) Shear Modulus and Damping in Soils: Measurement and Parameter Effects. *J. Soil Mech* **98**:603–624.

[8] Dostal L., Hollm M., Metrikine A. V., Tsouvalas A., van Dalen, K. N. (2021) Localized stationary seismic waves predicted using a nonlinear gradient elasticity model. *Nonlinear Dyn.* **107**:1107-1125.